CIMAC CONGRESS 25
ZURICH, MAY 19 – 23, 2025

2025 | 022

Potential problems of ammonia fuel engines within the tribological perspective

Tribology

Xing Xu, Harbin Engineering University

Xuan Ma, Harbin Engineering University
chang ge, Harbin Engineering University
Baofeng zhang, Harbin Engineering University
Xiqun LU, Harbin Engineering University

ABSTRACT

As a hydrogen-rich carbon-free fuel, ammonia fuel has attracted great attention in the engine field recently. However, there are few references available for investigating the tribological behaviors of the ammonia-fueled engine, which limits its development. For this purpose, the cylinder liner-piston ring (CLPR) was chosen as the research object for it is one of the most important friction pairs in the engine. And a systematic research strategy for the study of the tribological behaviors of CLPR in the ammonia-fueled engine is conducted. Based on the combustion performances of ammonia fuel, the inherent structural characteristics of the engine and the multi-lubrication state of the CLPR, the action mechanism of ammonia on the tribological behaviors of the CLPR can be explored from three levels.

The first is Extreme Boundary 1. Three typical working conditions are established, such as in the dry friction, the water medium and the ammonia solution medium. The effects of ammonia and ammonia solution on the tribological behavior and the surface damage of CLPR are clarified through a comparative study.

The second is the Extreme Boundary 2. The effects of the water and the ammonia solution on the lubricating oil are considered. The action mechanism of the ammonia and the ammonia solution on the physico-chemical performances and lubrication properties of the lubricating oil is analyzed.

The last one involves Multiple Conditions. Based on the results of Extreme Boundary 1 and Extreme Boundary 2, the dynamic influence mechanism between the water, the ammonia fuel and the lubricating oil are analyzed. And the multi-factor coupling research for the tribology (friction, wear and lubrication) of the CLPR is carried out accordingly.

The above research strategy can systematically study the tribological behaviors of CLPR in the ammonia-fueled engine under different working conditions. The results of Extreme Boundary 1 and Extreme Boundary 2 can guide and explain the research of Multiple Conditions. Meanwhile, the complex tribological behaviors of the CLPR in the ammonia-fueled engine can be decoupled by this method. Overall, this study serves as a foundational contribution to the field of tribology in ammonia fuel engines.

1 INTRODUCTION

The development of "low/zero carbon" fuels for the engine is driven by the stringent requirements on emissions [1]. To meet the need of greenhouse gas (GHG) emissions reduction, the transition of the engine fuel from fossil to low/zero-carbon fuels is necessary. Ammonia fuel, as a kind of zero-carbon fuel, can reduce GHG emissions [2]. When it combusts, some intermediates (NH_2, NH, HNO, NO, NNH, and N_2O) can be generated and the final products of the complete combustion are N_2 and H_2O, which is different from conventional fuels [3]. Meanwhile, the unburned fuel, combustion products, and intermediate products may appear in the engine because of its structural characteristics, which have a great influence on the performance of the engine [4].

The current researches of the ammonia-fueled engine mainly focus on injection strategies, ignition behaviors, and exhaust gas aftertreatment [5]. However, few researches about the tribological properties of the ammonia-fueled engine have been reported [6]. The ammonia-fueled engine is different from the conventional engine based on hydrocarbon fuels, so the study on the tribological properties of the ammonia-fueled engine is important. For conventional engines (such as vehicle diesel engines or heavy-duty diesel engines), 4% to 15% of the total fuel energy is used to overcome friction during the operation of moving parts. Within the typical friction losses, 7% to 15% of the energy is provided for the crankshaft system, while 20% to 30% for the valve mechanism and 40% to 55% for the cylinder liner-piston ring (CLPR) [7]. Numerous studies have been conducted on the tribological properties of conventional engines to develop a dvanced lubrication strategy, which can be a guide for the design and manufacture of the traditional engine [8]. An advanced lubrication strategy of the traditional engine can not only ensure high reliability and long service life of the ship, but also enhance the performance and reduce power loss of the ship, leading to a reduction in GHG emissions during the life cycle of the ship [9].

In addition, the lubrication strategy of the engine also needs to be adjusted to meet the challenges of fuel switching [10]. In the LNG engine, lubricants require higher ash content, and the tribological properties of the CLPR at high temperatures also need to be considered. In the methanol engine, the impact of methanol fuel and its combustion products on the tribological properties of the engine need to be investigated, particularly focusing on the tribocorrosion of the CLPR [11]. In the ammonia-fueled engine, the ammonia fuel has a certain corrosiveness, which can cause the stress corrosion cracking (SCC) of the metal [12], while the SCC can be mitigated by adding water (0.1 wt%-0.5 wt%) into ammonia fuel [13]. However, ammonia can easily combine with water to form the ammonia solution, which can corrode metal. Besides, water can be introduced by multiple ways, including the ammonia fuel itself, its combustion products, and scavenging processes [14]. Moreover, the start-stop condition of the engine could increase the possibility of the water. As a result, the effect of ammonia solution cannot be ignored as well, which can be inferred from the previous research of the traditional engine that ammonia solution may be formed in the upper part of the cylinder liner [15]. Therefore, the tribological properties of the ammonia-fueled engine need to be thoroughly assessed, if ammonia is to be used as a fuel.

As one of the most important friction pairs in the engine, the CLPR is selected as the research object. As shown in Fig.1, a systematic research

strategy is established to study the tribological behaviors of the CLPR in the ammonia-fueled engine. Based on the combustion performances of ammonia fuel, the inherent structural characteristics of the engine, and the multi-lubrication state of the CLPR [16], the action mechanism of ammonia on the tribological behaviors of the CLPR can be explored from three levels.

(1) The first level is Extreme Boundary 1. Three typical working conditions are established, including the dry friction, the water medium, and the ammonia solution medium. The effects of ammonia and ammonia solution on the tribological behaviors and the surface damage of CLPR are clarified through a comparative study.

(2) The second level is the Extreme Boundary 2. It considers the effects of the water and the ammonia solution on the lubricating oil. The action mechanism of the ammonia and the ammonia solution on the physico-chemical performances and lubricating properties of the lubricating oil is analyzed.

(3) The last one involves Multiple Conditions. Based on the results of Extreme Boundary 1 and Extreme Boundary 2, the dynamic influence mechanism between the water, the ammonia fuel and the lubricating oil are analyzed. And the multi-factor coupling research for the tribological properties of the CLPR is carried out in the situation that the practical working conditions in engines can be simulated. The multiple factors contain the change of temperature, pressure, and so on.

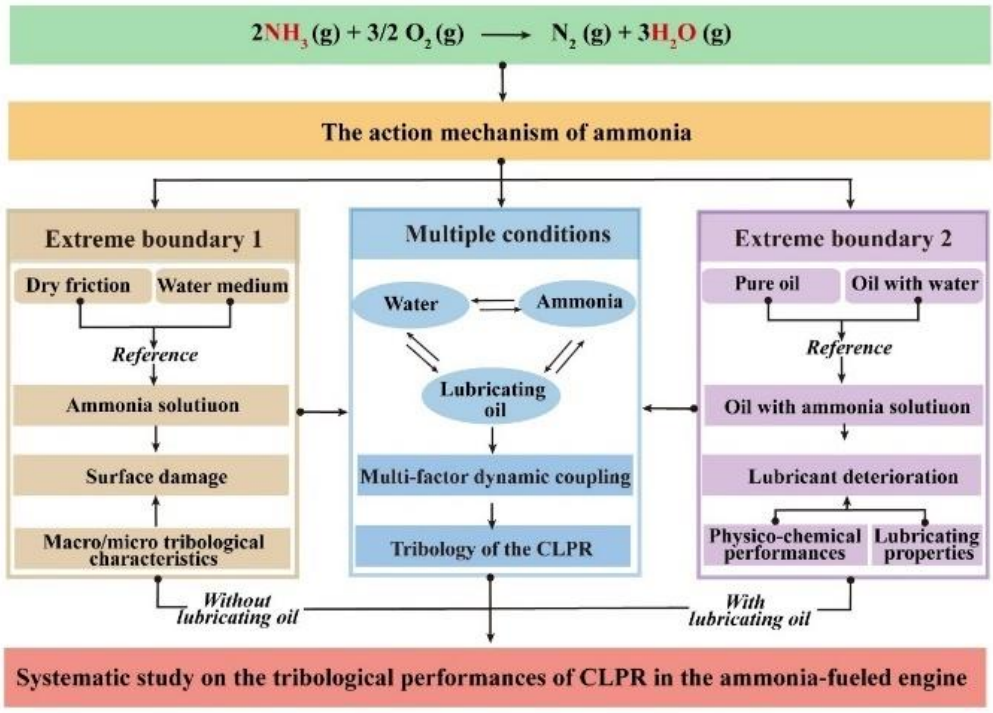

Fig.1 A systematic research strategy to study the tribological behaviors of CLPR in the ammonia-fueled engine.

This research strategy can systematically study the tribological behaviors of CLPR in the ammonia-fueled engine under different working conditions. And the results of Extreme Boundary 1 and Extreme Boundary 2 can be a guide for the research conducted under Multiple Condition.

Meanwhile, the complex tribological behaviors of the CLPR in the ammonia-fueled engine can be decoupled by this strategy. Studies of other extreme boundary are available from our published literature[17-18]. In this work, we mainly show the extreme boundary 2 part.

2 EXPERIMENTAL

2.1 Materials

The lubricating oil was one type of fully formulated oil, and the key additive components in the lubricating oil are shown in Table 1. The distilled water was provided by the laboratory, and the ammonia solution (25%, AR) was purchased from Shanghai Macklin Biochemical Technology Co., Ltd.

Table 1. The components of lubricating oil

Components	Content (wt%)
Base oil	>86.00
Zinc Dialkyldithiophosphates (ZDDP)	<1.00
Overbased calcium phenate (OCP)	<1.00
Others*	<12.00

To investigate the impact of ammonia on the tribological characteristics of lubricating oil, three distinct lubricating oil samples were formulated, with their specific compositions detailed in Table 2. All lubricating oil was stirred at 300 r/min for 10 mins before being used. The physicochemical properties of the three lubricating oils can be obtained from our previous study [18].

Table 2. The components of lubricating oil

Sample code	Lubricating oil (wt%)	Water (wt%)	Ammonia-water (wt%)
P-O	100.00	-	-
W-O	95.00	5.00	-
N-O	95.00	-	5.00

The cylinder liner-piston ring (CLPR) was used as friction pairs in the friction test. The friction pairs were cut from a new cylinder liner and piston rings using an electric spark wire-cutting machine. As shown in Fig. 1, the cylinder liner had dimensions of 30×10×6 mm (L×W×H), and the piston ring was processed into a 15 mm ring section. The cylinder liner was polished to avoid the influence of surface roughness, using 400#, 1000#, 2000#, and 3000# diamond sandpaper, along with a polishing solution to grind the samples. The surface roughness of the piston ring was Sa ≤ 0.2, and the surface roughness of the cylinder liner was Sa ≤ 0.1. Before conducting the friction test, all CLPR specimens underwent an ultrasonic cleaning procedure in ethanol for 10 minutes.

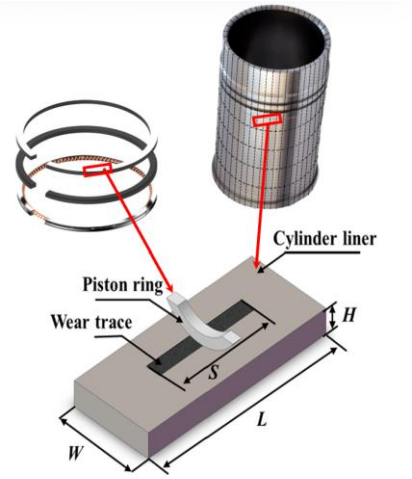

Fig. 1 The diagram of the piston ring and cylinder liner sample

2.2 Characterization

The tribological properties of various lubricating oils were tested using a tribometer (UMT Tribolab, Bruker, Germany), with average coefficients of friction (COF) recorded under different conditions. During the tribological test, the piston ring is secured in the upper fixture and remains stationary, while the cylinder liner is fixed in the lower fixture and undergoes reciprocating

motion. A vertical downward load is applied to the cylinder liner via the piston ring.

The three-dimensional topography of the surface was performed using a white light interferometer (DCM8, Leica, Germany), by which the wear volume (V_w), wear depth, and wear track width of the samples can be acquired directly. The wear rate (W) can be calculated from the wear volume loss by Eq. (1).

$$W = V_w / (P \bullet S) \quad (1)$$

where W is the wear rate (mm3/N·m), V_w is the wear volume loss (mm^3), P is the applied normal load (N), and S is the sliding distance (m).

The wear tracks were observed and analyzed by the digital microscope (DVM6A, Leica, Germany) and the scanning electron microscope (SEM, VEGA, Czech). The surface element distribution was characterized via energy dispersive spectroscopy (EDS, Bruker, Germany).

The hardness and elastic modulus of the cylinder liner were tested by the nanoindentation instrument (Hysitron TI Premier, Bruker, America) with a Berkovich indenter. The load and depth of penetration were independently measured by two sensors. The nanoindentation test is operated in a load control mode, with a fixed depth of 80 nm.

The chemical states of the elements on the worn surface were characterized by X-ray photoelectron spectroscopy (XPS, Thermo Scientific K-Alpha, America). Briefly, as the tribofilm is expected to have oxygen, sulfur, carbon, zinc, and possibly iron, all these elements were scanned. The acquired signals were collected from O1s, S2p, C1s, Zn2p and Fe2p. Before doing curve fitting, all the peaks were calibrated by shifting C 1s to 284.8 eV.

2.3 Method

The in-cylinder pressure curve and the piston ring velocity curve of a certain engine are shown in Fig. 2(a). Due to the influence of in-cylinder pressure and piston ring movement in the engine, boundary lubrication, mixed lubrication, and hydrodynamic lubrication may occur during the compression or working stroke between the piston ring and cylinder liner[20]. As shown in Fig. 2(b), the lubrication regime of friction pairs can be estimated by the film thickness ratio (λ), which is the ratio of the composite root-mean-square (RMS) roughness to the average film thickness. The wear of the CLPR mainly occurs in the boundary and mixed lubrication regimes[21, 22]. Therefore, this study focuses on the tribological characteristics of contaminated lubricating oil within these lubrication regimes.

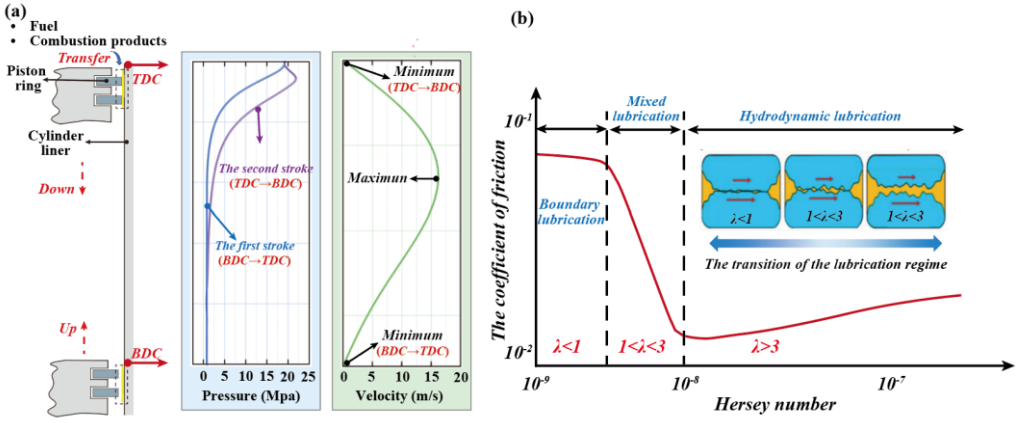

Fig. 2 (a) The cylinder pressure curve and the piston ring velocity curve of a certain engine, (b) the stribeck curve

The Hamrock-Dowson formula (Eq. 2) was used to calculate the minimum lubricant film thickness. The RMS roughness and λ were calculated using Eq. 3 and Eq. 4, respectively[23-25].

$$H_{min}^{*} = 3.63 \cdot R \cdot (G^{*0.49} \cdot U^{*0.68}) / W^{*0.073} \cdot (1 - e^{-0.68}) \quad (2)$$

$$\lambda = h_{min} / \sigma_{com} \quad (3)$$

$$\sigma_{com} = \sqrt{\sigma_1^{\,2} + \sigma_2^{\,2}} \quad (4)$$

Where $H_{min}^{*} = h_{min} / R$, $G^{*} = \alpha E'$, $U^{*} = \eta_0 \cdot U / (E^{'} \cdot R)$, $W^{*} = W / \left(E^{'} \cdot R^2\right)$, R is the radius of the piston ring, η is the oil viscosity, W is the applied load, σ1 is roughness of the piston ring, and σ2 is roughness of the cylinder liner. E′ denotes the equivalent elastic modulus, which can be calculated using Eq. (5), and U is the relative sliding speed, which can be determined from Eq. (6)

$$1 / E^{'} = (1 - v_1^{\,2}) / E_1 + \left(1 - v_2^{\,2}\right) / E_2 \quad (5)$$

$$U = V_{max} = \pi \cdot f \cdot 0.005 \quad (6)$$

Where f is frequency, v1 is the Poisson's ratio of the piston ring, E1 is the elastic modulus of the piston ring, and v2 is the Poisson's ratio of the cylinder liner, E2 is the elastic modulus of the piston ring. The essential parameters are shown in Table 3.

Table 3. The essential parameters

Parameter	Value
Cylinder liner radius (R)	0.17 (m)
Roughness of the piston ring (σ1)	0.20 (μm)
Roughness of the cylinder liner (σ2)	0.10 (μm)
Poisson's ratio of piston ring (v1)	0.27
Poisson's ratio of cylinder liner (v2)	0.27
Elastic modulus of piston ring (E1)	157.00(GPa)
Elastic modulus of piston ring (E2)	157.00(GPa)

Table 4. The parameter of the friction test

Sample code	Working condition		
	Load (N)	Frequency (Hz)	λ
P-O 100N-1Hz	100	1	0.238
P-O 100N-10Hz	100	10	1.143
P-O 500N-1Hz	500	1	0.212
P-O 500N-10Hz	500	10	1.017
W-O 100N-1Hz	100	1	0.281
W-O 100N-10Hz	100	10	1.345
W-O 500N-1Hz	500	1	0.251
W-O 500N-10Hz	500	10	1.197
N-O 100N-1Hz	100	1	0.789
N-O 100N-10Hz	100	10	3.779
N-O 500N-1Hz	500	1	0.702
N-O 500N-10Hz	500	10	3.361

According to the Hamrock-Dowson formula and laboratory conditions, the parameters for the friction test were set as shown in Table 4. Under a load of 500 N/100 N at 1 Hz, the λ for both P-O and W-O is less than 1, indicating a boundary lubrication regime. Under a load of 500 N/100 N at 10 Hz, the λ for both P-O and W-O is greater than 1 but less than 3, indicating a mixed lubrication regime. The lubrication regime of the N-O is similar to that of the P-O and W-O under a load of 500 N/100 N at 1 Hz, while the N-O exhibits a hydrodynamic lubrication regime under a load of 500 N/100 N at 1 Hz. This is because the viscosity

of N-O is much higher than that of P-O and W-O (Table 5). However, the previous study shows that the viscosity-temperature characteristic of N-O is degraded[18], and it may enter the mixed lubrication regime due to the flash temperature and frictional heat generated during the test.

Table 5. The viscosity of different lubricating oil

Sample code	Viscosity at 40℃ (mPa • s)
P-O	121.21
W-O	154.23
N-O	703.36

3 RESULTS AND DISCUSSION

3.1 The coefficient of friction

Fig. 3 shows the average COFs of different lubricating oils. Overall, the COF increases with load and decreases with frequency. This trend aligns with classical lubrication theory [26]. An increase in frequency can enhance the bearing capacity of the lubricating oil, thereby reducing the COF. In contrast, a higher load increases the motion resistance between the friction pairs, leading to a rise in the COF.

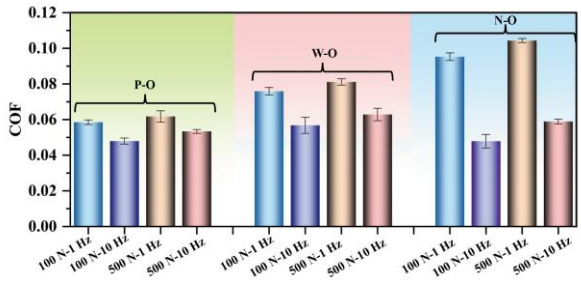

Fig. 3 The average COF of different lubricating oils

As shown in Fig. 4 (a) and (c), the COF of N-O was the highest, followed by W-O, while the COF of P-O was the lowest at a frequency of 1Hz, regardless of whether the load was 100 N or 500 N. This phenomenon may be attributed to differences in the lubricating oil viscosity. As mentioned earlier, the viscosity of N-O was the highest, followed by W-O, whereas P-O had the lowest viscosity, corresponding to its lowest COF. This could be due to the higher viscosity increasing motion resistance of the friction pair at low sliding frequencies, resulting in a higher COF.

Fig. 4 (b) show that under the 100 N-10 Hz, the COF curves of P-O, W-O, and N-O were close to each other, compared to the 100 N-1 Hz case. Similarly, Fig. 4 (d) show that the 500 N-10 Hz, the COF curves of P-O, W-O, and N-O were also close, compared to those of the 500 N-1 Hz. This suggested that the influence of viscosity on the COF of N-O was small at 10 Hz. The high-frequency reciprocating motion could result in an increase in the lubricating oil temperature, which caused the viscosity of N-O to be reduced. This also indicated that the P-O, W-O, and N-O may be in the same lubrication regimes (mixed lubrication regime) at the same load under 10 Hz.

In addition, the COF of N-O decreased more significantly than that of P-O and W-O, when the frequency increased from 1 Hz to 10 Hz with the same load. This also shows that the viscosity of the lubricating oil is a key parameter in determining the COF. Notably, the change in COF of the N-O also suggests that ammonia engines may experience greater power loss when started at low temperatures, leading to wasted energy. The results indicated that N-O had lubrication capabilities similar to P-O and W-O, and it retained the essential properties of liquid lubricating oil.

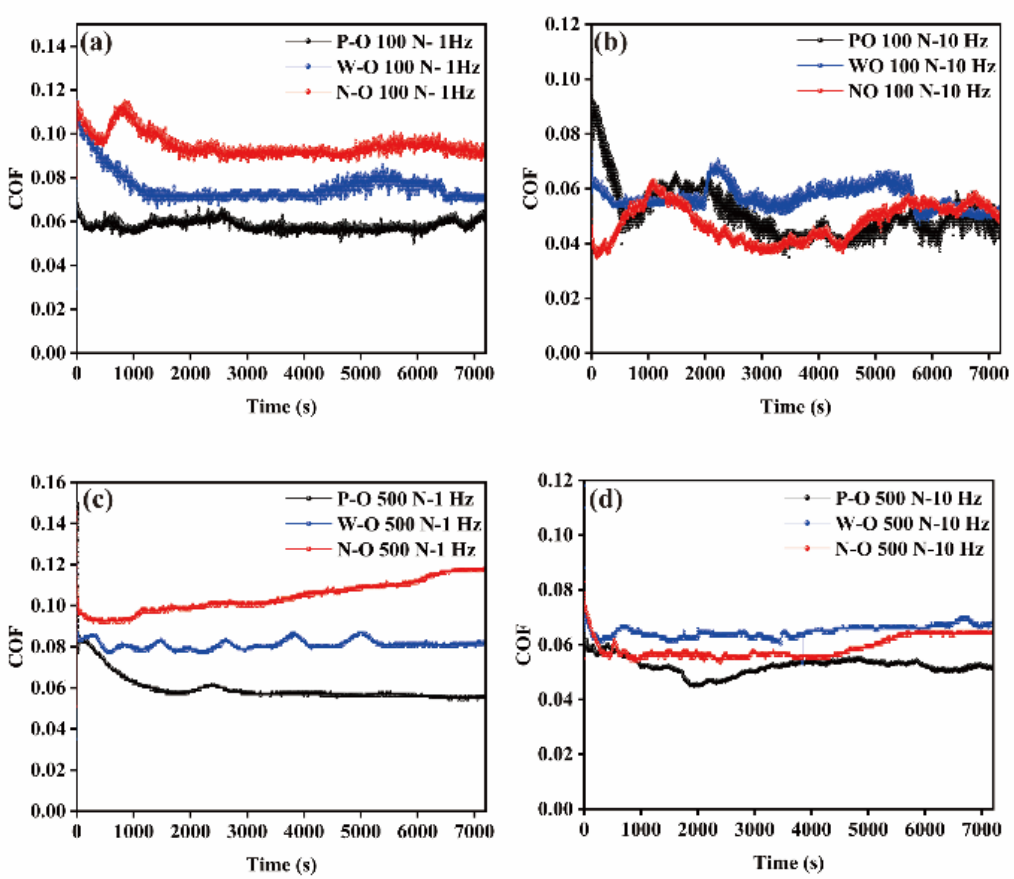

Fig. 4 The COF curves of P-O, W-O, and N-O under different working conditions, (a) 100 N-1 Hz, (b) 100 N-10Hz, (c) 500 N-1 Hz, and (d) 500 N-10 Hz

3.2 The wear characteristics of CLPR

To investigate the anti-wear performance of different lubricating oils, the wear tracks of the cylinder liner were analyzed by the white light interferometer. The representative topography of the wear tracks is shown in Fig.5, and the cross-sectional outlines were acquired. Whether under light load–high frequency or heavy load–low frequency conditions, the wear width and the wear depth of the cylinder liner with N-O lubrication was the most severe, followed by W-O, with the wear of the cylinder liner lubricated by P-O being the least severe. This meant that the anti-wear performance of the lubricating oil was influenced by ammonia solution and water.

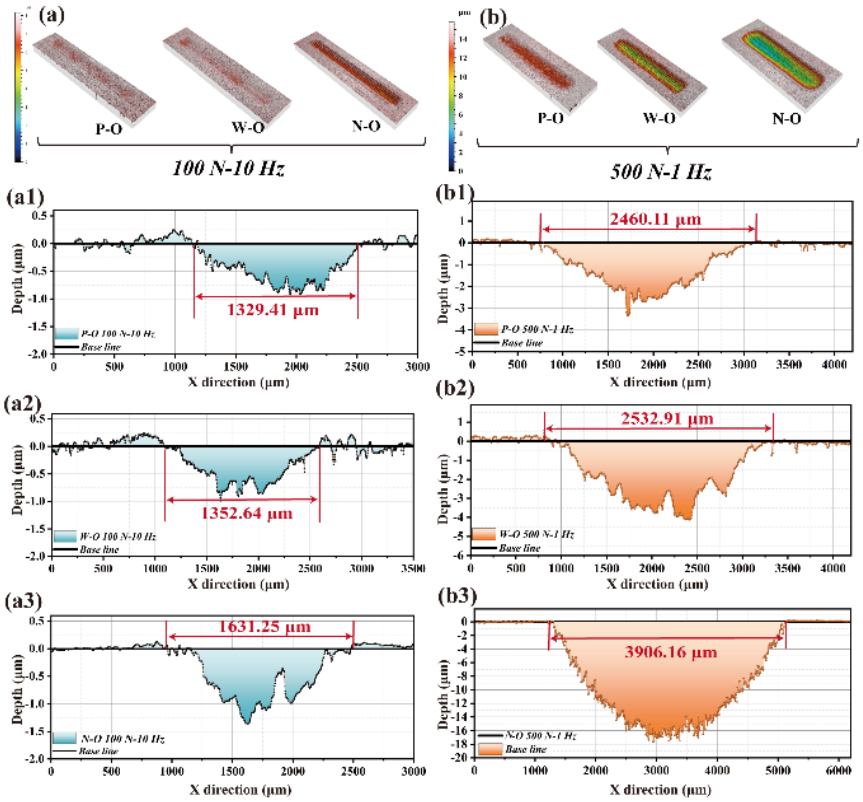

Fig. 5 Topography and cross-sectional outlines of the wear tracks in different lubricating oils: (a) topography and (a1)–(a3) cross-sectional outlines under 100 N–10 Hz; (b) topography and (b1)–(b3) cross-sectional outlines under 500 N–1 Hz

Fig.6 illustrates the wear rate of the cylinder liner. When the same lubricating oil was used, the wear rate increased with load but decreased with frequency. This can be attributed to higher loads causing greater surface damage, while increased frequency enhances the bearing capacity of the lubricating oil film, ultimately reducing the wear rate. Comparing the wear rate of different samples, it was clear that the wear rate of W-O and N-O consistently exceeded those of P-O, and this difference became more pronounced as the load increased. The variation trend of the wear rate was inconsistent with that of the COF. This was because the wear behavior of CLPR was influenced not only by the mechanical action of friction but also by the tribochemical reaction of the lubricating oil. In particular, at 500 N-1 Hz, the wear rate of the W-O increased by 63.57% compared to the P-O, while the wear rate of the N-O demonstrated a significant increase of 570.03%. However, regardless of the lubricant used, the lubrication regime of CLPR was identified as the boundary lubrication when the load was 500 N and the frequency was 1 Hz. Under the boundary lubrication regime, the influence of lubricating oil viscosity on the wear was small [27]. Consequently, it was difficult to fully attribute the variation in cylinder liner wear rate to the differences in viscosity among the lubricating oils.

Under the boundary lubrication regime, the wear behavior of the friction pair surface is influenced by the effects of lubricating oil additives. These additives can trigger tribochemical reactions on the worn surface under the action of temperature and load, leading to the formation of a boundary

lubrication film that reduces wear. As previously mentioned, the lubricating oil used in this study contains ZDDP (Table 1). ZDDP is commonly employed to enhance the anti-wear properties of lubricating oils. Consequently, the effectiveness of ZDDP in the W-O and N-O may be influenced, resulting in differences in wear behaviors among the P-O, W-O, and N-O.

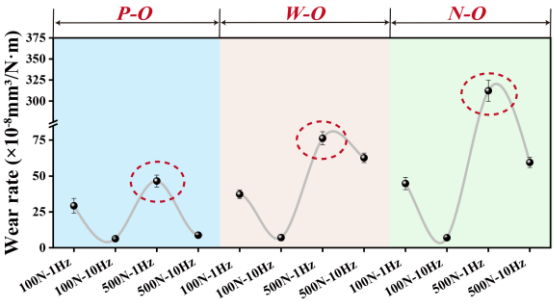

Fig. 6 The wear rate of the cylinder liner under different working conditions

3.3 The morphology of the worn surface

SEM was carried out on the cylinder liner's worn surface under different working conditions with P-O lubrication. For the P-O 100 N-1 Hz (Fig.7 (a)), the initial machining morphology and graphite can be observed on the worn surface, indicating that the wear of the cylinder liner surface was minimal. The morphology of the worn surface under the P-O 100 N-10 Hz was similar to that of the P-O 100 N-1 Hz. with only scratches observable. When the load was increased to 500 N, spalling and cracks could be found on the worn surface, as illustrated in Fig.7 (c) and (d). These suggest that P-O provides excellent lubrication, with fatigue wear and slight abrasive wear identified as the predominant wear mechanisms affecting the cylinder liner surface under these conditions.

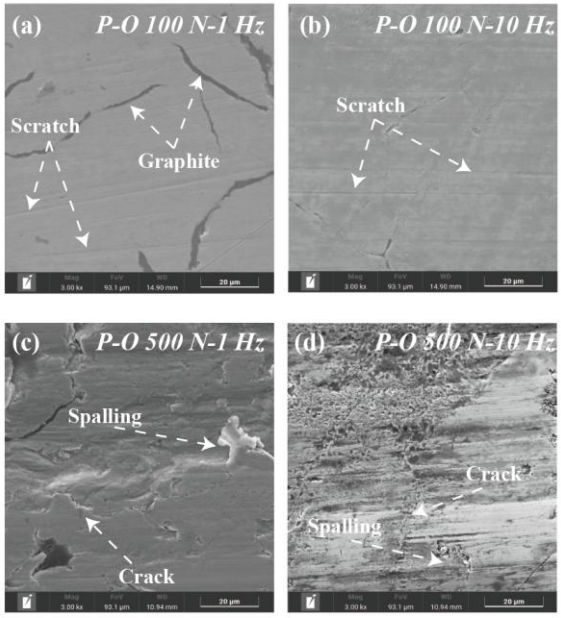

Fig. 7 SEM images of the cylinder liner's worn surface with P-O lubrication

Fig. 8 displays the morphology of the worn surface across various working conditions with W-O lubrication. Similar to the P-O 100N-1Hz, the initial machining morphology and graphite are also evident on the worn surface of the W-O 100N-1Hz. Furrows are observed on the worn cylinder liner at 100N-10Hz (Fig. 7(b)). In Fig. 7(c) and (d), spalling, particles, and furrows are visible on the worn cylinder liner. This result indicates that both abrasive wear and fatigue wear occur on the cylinder liner surface under W-O lubrication conditions.

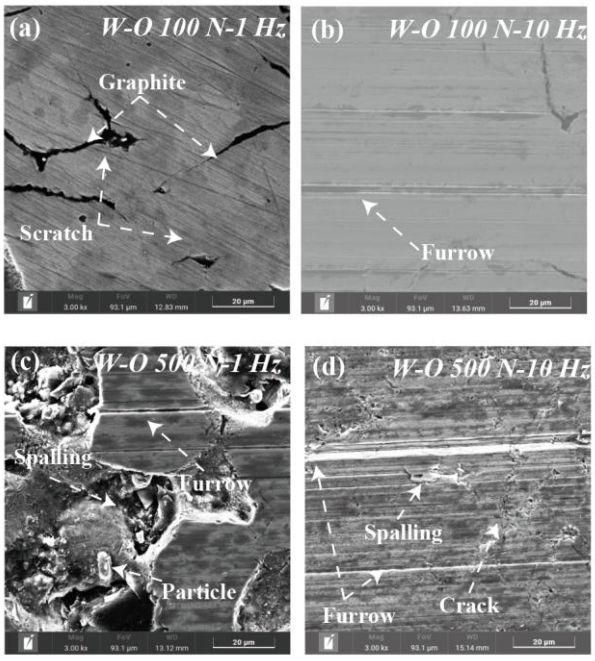

Fig. 8 SEM images of the cylinder liner's worn surface with W-O lubrication

As shown in Fig. 9, furrows, cracks, and particles could be seen on the worn surface of the cylinder liner with N-O lubrication. The wear mechanisms of the cylinder liner surface were abrasive wear and fatigue wear. Furthermore, compared to W-O and P-O lubrications, the furrows on the cylinder liner surface with N-O lubrication were more pronounced, regardless of whether the conditions were set at 100 N-1 Hz or 500 N-1 Hz. This observation indicated that the anti-wear property of N-O was inferior to that of P-O and W-O.

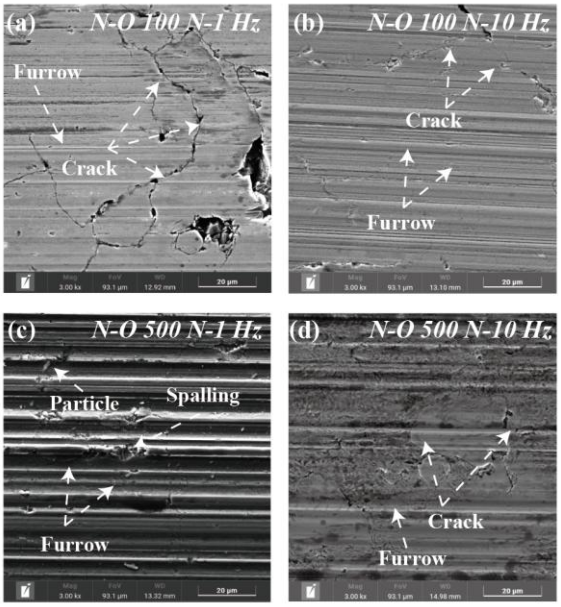

Fig. 9 SEM images of the cylinder liner's worn surface with W-O lubrication

3.4 The element distribution of worn surface

To further analyze the differences in anti-wear properties of the various lubricating oils, the elemental distribution on the worn surfaces of the cylinder liner and piston ring was collected, respectively. As illustrated in Fig. 10(a), the microstructure of the piston ring coating exhibited slight damage. The Fe element content of the worn piston ring surface was 1.22 wt%, with the majority of it located within the microstructure. This indicates that the wear on the piston ring also was minimal. Fig. 10(b) shows that the surface of the piston ring of the W-O 500 N-1 Hz was smoother compared to that of the P-O 500 N-1 Hz. Most of the microstructure of the piston ring surface was damaged at W-O 500 N-1 Hz, and the Fe element was uniformly distributed across the surface. It's worth noting that the surface microstructure of the piston ring at N-O 500 N-1 Hz was destroyed, leading to the formation of furrows. Analyzing the distribution of Cr and Fe elements suggests that the surface coating of the piston ring might be partially

damaged, resulting in the exposure of the underlying base material.

A comparative analysis of the oxygen (O) content across different worn surfaces reveals that the N-O lubricated surface has the lowest oxygen content, followed by the W-O surface, while the P-O surface has the highest oxygen content. Optical microscopy images support these findings (Fig. 11), indicating minimal oxide formation on the P-O surface subjected to 500N at 1 Hz, more oxide on the W-O surface under the same conditions, and nearly complete oxide coverage on the N-O surface. During testing, iron reacts with oxygen due to frictional heat, and further corrosion of the cylinder liner occurs from exposure to water and ammonia solutions, leading to an increased oxygen content on the surface.

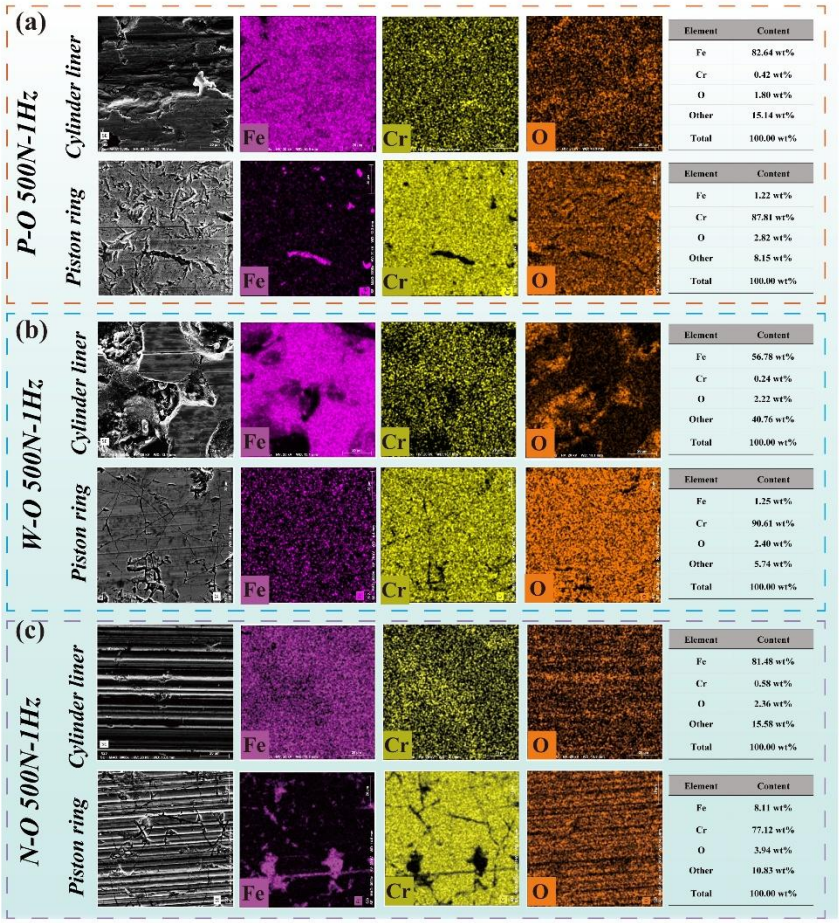

Fig. 10 The elemental distribution on the worn surfaces of the cylinder liner and piston ring, (a) P-O 500 N-1 Hz, (b) W-O 500 N-1 Hz, and (c) N-O 500 N-1 Hz

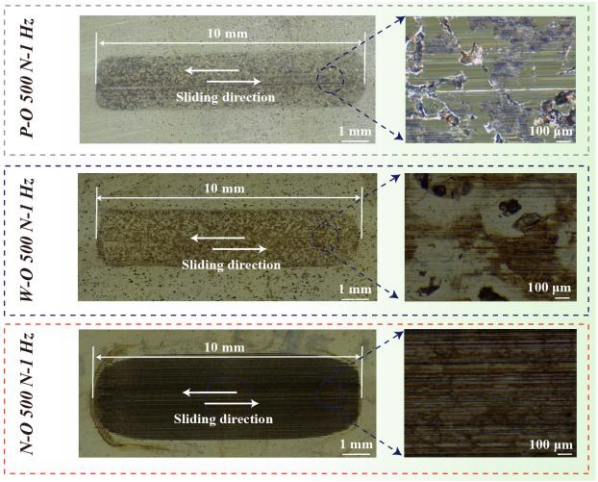

Fig. 11 The optical microscope photograph of the worn cylinder liner surface

The distribution of Zn elements was analyzed to examine the formation of the tribochemical reaction film on the worn surface, as illustrated in Fig. 12. Under both boundary and mixed lubrication regimes, the anti-wear performance of the fully formulated commercial lubricating oil relies on the development of this tribochemical film on the worn surface [28, 29]. Fig. 12 shows that a tribochemical reaction film could form on most of the worn surfaces under P-O and W-O lubrication conditions. However, the Zn element was not found on the worn surface at P-O/W-O 100 N-1 Hz, likely because the working conditions did not trigger the development of the tribochemical reaction film. Notably, no Zn element was found on the worn surface under N-O lubrication, regardless of the working conditions. This suggests that no tribochemical reaction film formed on the worn surface of the cylinder liner. Consequently, it also means that ZDDP in the N-O might have failed.

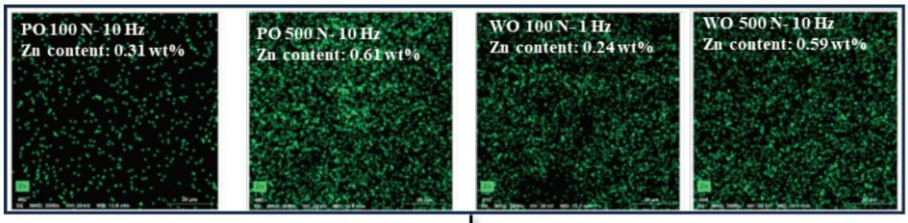

Zn elements content (wt%)

Oil	Working conditions			
	100 N-1 Hz	100 N-10Hz	500 N-1 Hz	500 N-10 Hz
P-O	? (0.05)	√ (0.31)	√ (0.54)	√ (0.61)
W-O	×	√ (0.24)	√ (0.38)	√ (0.59)
N-O	×	×	×	×

Fig. 12 The distribution and content of the Zn elements on the worn surface of the cylinder liner

3.5 The influencing mechanism of different lubricating oil

To investigate the wear mechanisms of the cylinder liner, nanoindentation was employed to characterize the mechanical properties of the worn surface. Since the CLPR operated under reciprocating sliding conditions, sample points were selected at the head, middle, and tail of the wear track, as shown in Fig.13 (a). Fig.13 (b)–(e) display the Young's modulus (Er) and hardness of the different surfaces. The results indicate that Young's modulus and hardness of the cylinder liner

surface under P-O 500N-1Hz and W-O 500N-1Hz conditions were lower than those of the original surface. This can be attributed to the tribochemical film on the worn surface of the cylinder liner, which results in lower Young's modulus and hardness [30].

However, compared to the original surface, Young's modulus and hardness of the worn cylinder liner surface under N-O 500N-1Hz were reduced by 94.08% and 91.02%, respectively. Moreover, Young's modulus and hardness of the worn cylinder liner surface under N-O 500N-1Hz were also significantly lower than those under P-O 500N-1Hz and W-O 500N-1Hz. According to Achard's wear theory [26], the wear of friction pairs is inversely proportional to the mechanical properties of the material, particularly in the case of abrasive wear, as shown in Eq. (7).

$$\frac{dv}{ds} = k_a \cdot \frac{W}{H} \qquad (7)$$

Where $\frac{dv}{ds}$ is the unit volume wear, ka is the abrasive wear constant, H is the material hardness, and W is the load. Therefore, the increased wear of the cylinder liner with N-O lubrication may be attributed to a reduction in the mechanical properties of its surface.

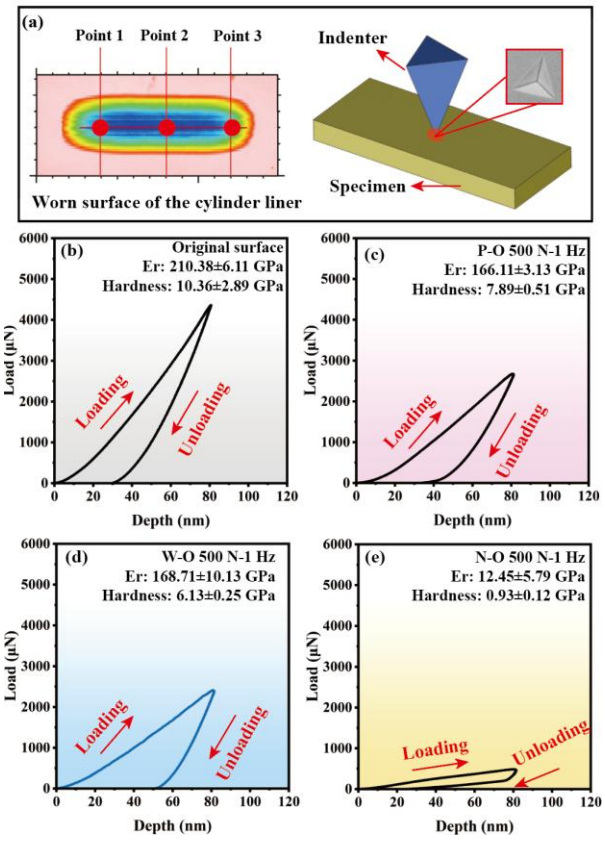

Fig. 13 (a) Sample point for nanoindentation on the worn surface of the cylinder liner, Young's modulus and hardness of the different surface at (b) original surface, (c) P-O 500 N-1 Hz, (d) W-O 500 N-1 Hz and (e) N-O 500 N-1 Hz

In order to further clarify the anti-wear performance of different lubricating oils, XPS was applied to confirm the chemical structure on the wear scar of the cylinder liner. The O1s signal appeared to comprise three main peaks (Fig. 14 (a)), corresponding to non-bridging oxygen (NBO), bridging oxygen (BO), and metal oxide (MO). In all the tribotests, the BO, NBO, and MO were identified at 533.06 ± 0.2 eV, 531.76 ± 0.2 eV, and 530.36 ± 0.3 eV [28], respectively. Moreover, XPS analysis shows significant differences in BO/NBO. It can be seen that the BO/NBO ratio (0.18±0.01) of the worn surface with the N-O 500N-1Hz was unusually low. According to the theoretical BO/NBO (Table 6) of the various phosphate structures [28, 31], a high proportion of

pyrophosphate was found on the worn surface with the N-O 500N-1Hz.

Table 6. The theoretical BO/NBO of the various phosphate structures

	Ortho-	Pyro-	Poly-(6P)	Poly-(12P)	Meta-	Ultra-
BO/NBO	0	0.17	0.36	0.42	0.5	1.5

Fe 2p signal was broad as shown in Fig. 14 (b). Four peaks were fitted at 706.7± 0.2 eV, 709.6 ± 0.3 eV, 710.8± 0.2 eV and 714.0 ± 0.2 eV, corresponding to metallic iron, Fe(II) oxide, Fe(III) oxides, and Fe(II) satellite, respectively[28].

The one peak of S2p appeared at 161.5 ± 0.1 eV (Fig. 14 (c)), which was ascribed to metal sulfide (S Ⅳ). This suggested the formation of FeS or ZnS on the worn surface of the cylinder liner. Another S2p peak appeared at 169 ± 0.2 eV, which indicated the presence of sulfate ((S Ⅱ) on the worn surface of the cylinder liner[28, 32]. However, the XPS spectra revealed that metal sulfide was not formed on the worn surface at N-O 500 N-1Hz, which was different from the results observed at P-O 500 N-1Hz and W-O 500 N-1Hz.

Zn2p signal appeared at 1022.5 ± 0.1 eV corresponding to either zinc phosphate [28, 33], which is more probable, or ZnS, Zn(SO4), or ZnO, as shown in Fig 14 (d). Similar to the signal of S2p, no signal of Zn was found on the worn surface of the cylinder liner at N-O 500 N-1Hz.

By comparing the XPS spectra of different worn surfaces, the following points can be obtained:

(1) Under the condition of N-O lubrication, the formation of sulfide on the wear surface is inhibited. On the one hand, this blocks the reaction between ZDDP and the worn surface, so that the tribochemical reaction film cannot be formed, and on the other hand, the Zn element also cannot be deposited on the worn surface of the friction pair.

(2) Under the condition of N-O lubrication, a large number of short-chain phosphates were still formed on the worn surface, which indicated that the ammonia solution of N-O may destroy the exchange strategy of zinc ions and iron ions in the traditional ZDDP reaction.

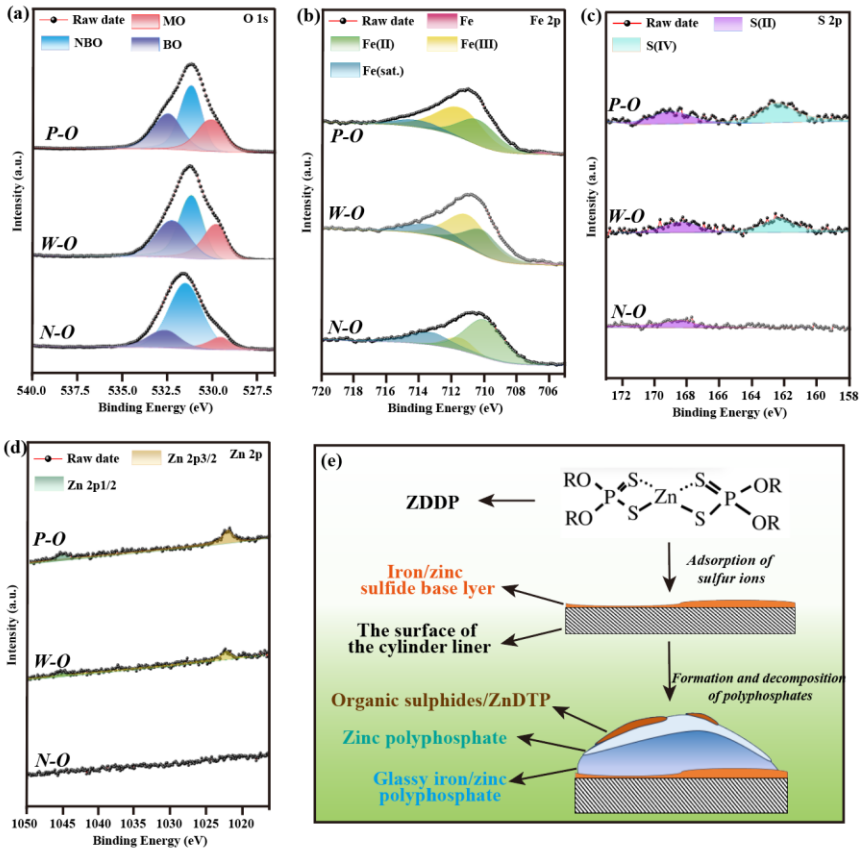

Fig. 14 High-resolution XPS spectra in different regions, (a) O1s region, (b) Fe2p region, (c) S2p region, (d) Zn2p region, and (e) schematic diagram of ZDDP film

According to the XPS results, ZDDP in P-O and W-O could form a tribochemical reaction film on the worn surfaces, while ZDDP in N-O failed to do so, and this finding was also consistent with the EDS results. The reaction mechanism of the tribofilm formed by ZDDP has been extensively studied [28, 29, 33-36], as illustrated in Fig. 14(e). The initial stage involves the diffusion and adsorption of ZDDP molecules onto the friction surface, where they adsorb onto Fe through the sulfur atoms of the P=S bond. Following adsorption, an intermolecular reaction between dialkyl dithiophosphate (or dithioalkyl phosphate) species occurs, leading to rapid polymerization and the formation of long-chain polyphosphates or metaphosphates. This is subsequently followed by a slower depolymerization of these long phosphate chains into shorter-chain phosphates. This process arises because the exchange of Zn2+ with Fe3+ needs more negative charges to balance the reaction [29, 34], and this requires a shortening of the chain length.

Moreover, the acid-base reaction between phosphate and iron stems from the fact that Fe3+ is a harder Lewis acid than Zn_2^+, and cation exchange is energetically advantageous from the perspective of Pearson's HSAB principle [29, 35]. Phosphates are hard bases that specialize in reacting with hard acids [34]. Additionally, it is important to note that the ammonia solution in N-O can ionize to produce NH_4^+. As NH_4^+ is also a Lewis acid, it may participate in the ZDDP reaction.

The above results indicate that the wear behavior of the cylinder liner under N-O lubrication was

significantly different from that observed under P-O and W-O lubrications. As shown in Fig.15, two potential mechanisms explain how ammonia solution influences the anti-wear properties of lubricating oil:

(1) Ammonia solution in N-O would trigger electrochemical reactions on the cylinder liner surface, resulting in galvanic corrosion [19, 37-39]. This corrosion may not only promote the active dissolution of Fe, but also form a loosely structured oxide layer, which weakens the mechanical properties of the surface and increases surface wear. Additionally, the oxide layer may contribute to abrasive wear on the friction pair surface, further exacerbating wear on the cylinder liner [10].

(2) The ammonia solution in N-O can be ionized, and produced ammonia ions that interfere with the acid-base reaction mechanism of ZDDP. As a result, ZDDP would not form a protective tribochemical film on the friction pair surface, leading to increased surface wear of the cylinder liner.

However, some studies have shown that severe abrasive wear may cause the tribochemical reaction film formed by ZDDP to detach from the surface [40], which could lead to the mutual promotion of mechanical wear and corrosion wear under N-O lubrication.

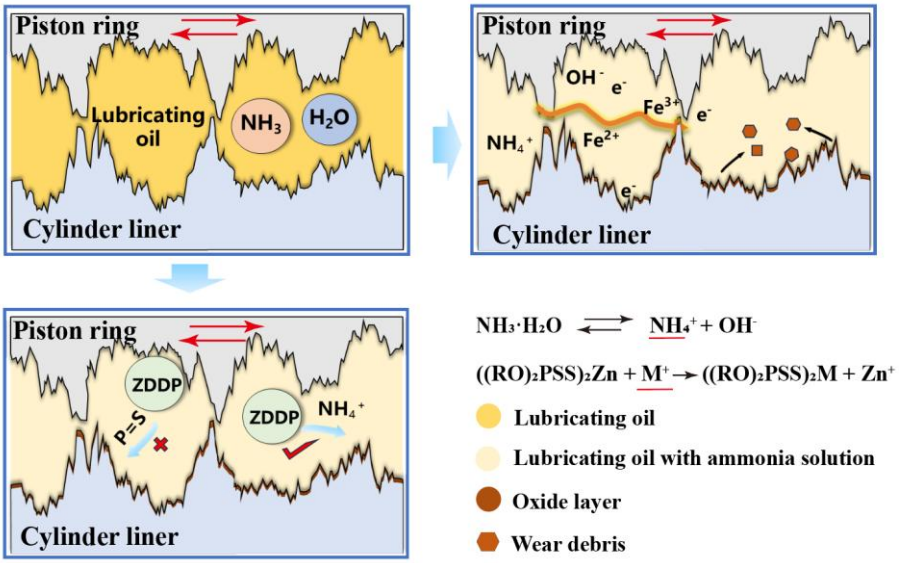

Fig. 15 Diagram of wear mechanism of cylinder liner under N-O lubrication condition

4 CONCLUSIONS

In this study, the tribological properties of contaminated lubricating oil in the ammonia-fueled engine were investigated through a comparative analysis. Three different lubricants—P-O, W-O, and N-O—were artificially prepared for this purpose. The CLPR was used as the friction pair, and the friction coefficient, wear rate, and worn morphological characteristics of CLPR under different lubrication conditions were analyzed. The mechanisms affecting the tribological properties of the lubricating oil were also explored. The major conclusions of the studies described above are listed below.

(1) The influence of different lubricating oils on the CLPR's friction coefficient is reflected in the

difference in lubricating oil viscosity. On the one hand, the high viscosity of N-O provides better oil film bearing capacity at higher frequencies. On the other hand, it also increases the motion resistance of the friction pair.

(2) Both water and ammonia solution in lubricating oil would increase the surface wear of the cylinder liner, with the effect of ammonia solution being more significant than that of water.

(3) The presence of ammonia solution in the lubricating oil would corrode the cylinder liner, thereby degrading the mechanical properties of the cylinder liner surface. Additionally, the wear debris generated during this process may contribute to abrasive wear, further increasing the surface wear of the cylinder liner.

(4) The ammonium ions present in the ammonia solution disrupt the tribochemical reaction mechanism of ZDDP. Consequently, this interference prevents ZDDP from forming a tribochemical reaction film on the cylinder liner surface with the N-O lubrication, leading to increased wear on the cylinder liner surface.

5 ACKNOWLEDGMENTS

This work was supported by the Study on Tribology and Lubrication Technology of the Marine Low-Speed Engine (No. CBG5N21-1-2), the Tribological Design and Experimental Verification of Key Moving Parts (No. DE0305), the Study on the Key Technologies of Green Ammonia Synthesis and Engine Application, the Fundamental Research Funds for the Central Universities.

6 REFERENCES AND BIBLIOGRAPHY

[1] Lion S, Vlaskos I, Taccani R. A review of emissions reduction technologies for low and medium speed marine Diesel engines and their potential for waste heat recovery [J]. *Energy Conversion and Management*, 207: (2020)

[2] Lee H, Park D, Choo S, et al. Estimation of the Non-Greenhouse Gas Emissions Inventory from Ships in the Port of Incheon [J]. *Sustainability*, 12(19): 8231 (2020)

[3] El-Refaei SM, Russo PA, Pinna N. Recent Advances in Multimetal and Doped Transition-Metal Phosphides for the Hydrogen Evolution Reaction at Different pH values [J]. *ACS Applied Materials & Interfaces*, 13(19): 22077-22097 (2021)

[4] Mallouppas G, Ioannou C, Yfantis EA. A Review of the Latest Trends in the Use of Green Ammonia as an Energy Carrier in Maritime Industry [J]. *Energies*, 15(4): 1453 (2022)

[5] Kurien C, Mittal M. Review on the production and utilization of green ammonia as an alternate fuel in dual-fuel compression ignition engines [J]. *Energy Conversion and Management*, 251: 114990 (2022)

[6] Chiong M-C, Chong CT, Ng J-H, et al. Advancements of combustion technologies in the ammonia-fuelled engines [J]. *Energy Conversion and Management,* 244: 114460 (2021)

[7] Chehade G, Dincer I. Progress in green ammonia production as potential carbon-free fuel [J]. *Fuel*, 299: 120845 (2021)

[8] Bae C, Kim J. Alternative fuels for internal combustion engines [J]. *Proceedings of the Combustion Institute*, 36(3): 3389-3413 (2017)

[9] Tavakoli S, Jensen MV, Pedersen E, et al. Unburned hydrocarbon formation in a natural gas engine under sea wave load conditions [J]. *Journal of Marine Science and Technology*, 26(1): 128-140 (2021)

[10] Kidoguchi Y, Nada Y, Sangawa S, et al. Effect of low load combustion and emissions on fuel dilution in lubricating oil and deposit formation of DI diesel engines fueled by straight rapeseed oil [J]. *Fuel*, 221: 35-43 (2018)

[11] Xu X, Liu E, Zhu N, et al. Review of the Current Status of Ammonia-Blended Hydrogen Fuel Engine Development [J]. *Energies*, 15(3): 1023 (2022)

[12] Sahin Z, Akcanca IZ, Durgun O. Experimental investigation of the effects of ammonia solution (NH3OH) on engine performance and exhaust emissions of a small diesel engine [J]. *Fuel*, 214: 330-341 (2018)

[13] Wang B, Yang C, Wang H, et al. Study on injection strategy of ammonia/hydrogen dual fuel engine under different compression ratios [J]. *Fuel*, 334: 126666 (2023)

[14] Dong DS, Wei FX, Long WQ, et al. Optical investigation of ammonia rich combustion based on methanol jet ignition by means of an ignition chamber [J]. *Fuel*, 345: 128202 (2023)

[15] Agocs A, Rappo M, Obrecht N, et al. The Impact of Ammonia Fuel on Marine Engine Lubrication: An Artificial Lubricant Ageing Approach [J]. *Lubricants*, 11(4): 165 (2023)

[16] Wong VW, Tung SC. Overview of automotive engine friction and reduction trends–Effects of

surface, material, and lubricant-additive technologies [J]. *Friction*, 4(1): 1-28 (2016)
[17] Xu X, Ge C, Zhang B, et al. Study on the tribological behaviors of the cylinder liner-piston ring in the ammonia-fueled engine [J]. *Friction*, 2024.
[18] Xu X, Ge C, Zhang B, et al. The degeneration mechanism of lubricating oil in the ammonia fuel engine [J]. *Tribology International*, 2025, 202 110333.
[19] Rahmani R, Rahnejat H, Fitzsimons B, et al. The effect of cylinder liner operating temperature on frictional loss and engine emissions in piston ring conjunction. *Applied Energy,* 191: 568-581 (2017)

[20] Wopelka T, Cihak-Bayr U, Lenauer C, et al. Wear of different material pairings for the cylinder liner – piston ring contact [J]. *Industrial Lubrication and Tribology*, 2018, 70(4): 687-99.
[21] Zabala B, Igartua A, Fernández X, et al. Friction and wear of a piston ring/cylinder liner at the top dead centre: Experimental study and modelling [J]. *Tribology International*, 2017, 106 23-33.
[22] Bolander NW, Steenwyk BD, Sadeghi F, et al. Lubrication regime transitions at the piston ring-cylinder liner interface [J]. *Proceedings of the Institution of Mechanical Engineers Part J-Journal of Engineering Tribology*, 2005, 219(J1): 19-31.
[23] Bai L, Meng Y, Zhang V, et al. Effect of Surface Topography on ZDDP Tribofilm Formation During Running-in Stage Subject to Boundary Lubrication [J]. *Tribology Letters*, 2021, 70(1): 10.
[24] Ge C, Zhang B, Xu X, et al. Tribofilm distribution and tribological analysis of piston ring-cylinder liner interfaces under realistic engine conditions [J]. *Tribology International*, 2025, 201 110250.
[25] Xiuyi L, Jiao B, Lu X, et al. A statistical piston ring lubrication model considering the tribofilm and its effect of two-stroke marine engines [J]. *Tribology International*, 2023, 177 107996.
[26] Wen S, Huang P. Principles of tribology: *John Wiley & Sons*; 2017.
[27] Hsu SM, Gates RS. Boundary lubricating films: formation and lubrication mechanism [J]. *Tribology International*, 2005, 38(3): 305-12.
[28] Dorgham A, Azam A, Parsaeian P, et al. Understanding the effect of water on the transient decomposition of zinc dialkyldithiophosphate (ZDDP) [J]. *Tribology International*, 2021, 157 106855.
[29] Spikes H. The History and Mechanisms of ZDDP [J]. *Tribology Letters*, 2004, 17(3): 469-89.
[30] Sato K, Watanabe S, Sasaki S. High Friction Mechanism of ZDDP Tribofilm Based on in situ AFM Observation of Nano-Friction and Adhesion Properties [J]. *Tribology Letters*, 2022, 70(3): 94.
[31] Ueda M, Spikes H. ZDDP Tribofilm Formation and Removal [J]. *Tribology Letters*, 2024, 72(4): 109.
[32] Heuberger R, Rossi A, Spencer ND. XPS study of the influence of temperature on ZnDTP tribofilm composition [J]. *Tribology Letters*, 2007, 25(3): 185-96.
[33] Eglin M, Rossi A, Spencer ND. X-ray Photoelectron Spectroscopy Analysis of Tribostressed Samples in the Presence of ZnDTP: A Combinatorial Approach [J]. *Tribology Letters*, 2003, 15(3): 199-209.
[34] Martin JM, Grossiord C, Le Mogne T, et al. The two-layer structure of Zndtp tribofilms: Part I: AES, XPS and XANES analyses [J]. *Tribology International*, 2001, 34(8): 523-30.
[35] Minfray C, Martin JM, Esnouf C, et al. A multi-technique approach of tribofilm characterisation [J]. *Thin Solid Films*, 2004, 447-448 272-7.
[36] Soltanahmadi S, Morina A, van Eijk MCP, et al. Tribochemical study of micropitting in tribocorrosive lubricated contacts: The influence of water and relative humidity [J]. *Tribology International*, 2017, 107 184-98.
[37] JONES DA, WILDE BE. Corrosion Performance of Some Metals and Alloys in Liquid Ammonia [J]. *Corrosion*, 2013, 33(2): 46-50.
[38] Sun L, Xiong Z, Qiu J, et al. Corrosion behavior of carbon steel in dilute ammonia solution [J]. *Electrochimica Acta*, 2020, 364 137295.
[39] Cai Y, Wang Z, Tang Y, et al. Corrosion fatigue behavior of cast iron in simulated combustion product solutions of ammonia and methanol fuels [J]. *International Journal of Fatigue*, 2025, 191 108715.
[40] Agocs A, Frauscher M, Ristic A, et al. Impact of Soot on Internal Combustion Engine Lubrication—Oil Condition Monitoring, Tribological Properties, and Surface Chemistry [J]. *Lubricants*, 2024, 12(11): 401.